

Study of $\text{Ir}_x\text{Mn}_y(\text{CO})_n(\text{DMF})_z$ as Electrocatalyst for Oxygen Reduction and Hydrogen Oxidation in the Presence of Fuel Cell Contaminants

M.L. Barrios-Reyna¹, J. Uribe-Godínez^{1,3,†}, J.M. Olivares-Ramírez² and O. Jiménez-Sandoval^{1,*}

¹Centro de Investigación y de Estudios Avanzados del Instituto Politécnico Nacional,

Unidad Querétaro, Libramiento Norponiente 2000, Fracc. Real de Juriquilla, Querétaro, Qro. 76230, MEXICO.

²Universidad Tecnológica de San Juan del Río, Av. La Palma No. 125, Col. Vista Hermosa, San Juan del Río, Qro. 76800, MEXICO.

³Centro Nacional de Metrología, Km 4.5 Carretera a Los Cués, El Marqués, Qro. 76246, MEXICO.

Received: July 05, 2016, Accepted: October 15, 2016, Available online: November 04, 2016

Abstract: The oxygen reduction reaction (ORR) and the hydrogen oxidation reaction (HOR) have been studied on a wide range of electrocatalysts, including bimetallic materials which are based solely on platinum group metals and their alloys. This work reports the synthesis and characterization of a novel bimetallic electrocatalyst, $\text{Ir}_x\text{Mn}_y(\text{CO})_n(\text{DMF})_z$, for the ORR and HOR in acid media. The material was synthesized by reacting $\text{Ir}_4(\text{CO})_{12}$ and $\text{MnCl}_2 \cdot 4\text{H}_2\text{O}$ in DMF. It was characterized structurally by FT-IR and micro-Raman spectroscopy, X-ray diffraction, SEM and energy-dispersive X-ray spectroscopy; the electrochemical characterization was made by the rotating disk electrode technique, at room temperature. The electrocatalytic activity of the new material for the ORR and HOR does not show appreciable variations due to the presence of methanol or carbon monoxide, respectively, even at high concentrations of these contaminants (2 mol L⁻¹ methanol and 0.5% CO). This tolerance is a very important property with respect to platinum-based catalysts, which are poisoned by low concentrations of such contaminants. The kinetic parameters of the novel catalyst, such as Tafel slope (b), exchange current density (j_0) and charge transfer coefficient (α), are reported as well. The results show that the novel electrocatalyst is attractive for evaluation as cathode/anode in PEM fuel cells.

Keywords: Electrocatalyst, Oxygen Reduction Reaction, Hydrogen, CO-Tolerance, Methanol, PEM Fuel Cell

1. INTRODUCTION

A polymer electrolyte membrane fuel cell (PEMFC) is a device in which hydrogen and oxygen electrochemically react to produce electricity with water as the only by-product. Fuel cells offer the capability to provide clean energy transportation with zero carbon dioxide emissions [1].

PEMFCs currently use Pt as catalyst both at the cathode and the anode. However, this material presents serious disadvantages, such as: high cost and poor yield due to its easy deactivation by the action of molecules often present in the hydrogen fuel feed, such as carbon monoxide [2]. The high penetration of methanol into the platinum cathode compartment through the polymer membrane of the Direct Methanol Fuel Cell (crossover effect) is another prob-

lem which results in a significant loss of performance of this fuel cell [3, 4]. Therefore, it is necessary to investigate new materials that perform the oxygen reduction reaction (ORR) and hydrogen oxidation reaction (HOR) with high catalytic activity and tolerance to the presence of methanol and carbon monoxide, respectively. Pt-based alloy catalysts have shown enhanced activity towards oxygen reduction [5]. The improved activity of these modified Pt structures has been attributed to many factors including changes in the electronic properties of the catalyst surface [6]. Relatively few catalysts used as cathodes have been reported to show varying degrees of resistance to methanol, such as Pt-Se [7] and Pt-Ru [8]; however, most of these materials do not tolerate methanol concentrations above 1.0 mol L⁻¹. There are few works in which Mn is used as an electrocatalyst for PEMFCs. For example, Pt-Mn has been synthesized by different methods [9, 10] and its important ORR activity reported. On the other hand, there are several studies of iridium based electrocatalysts used as cathodes in fuel cells [11-

To whom correspondence should be addressed:
Email: *ojimenez@cinvestav.mx, † juribe@cenam.mx
Phone: +52-442-2119900, Fax: +52-442-2119938

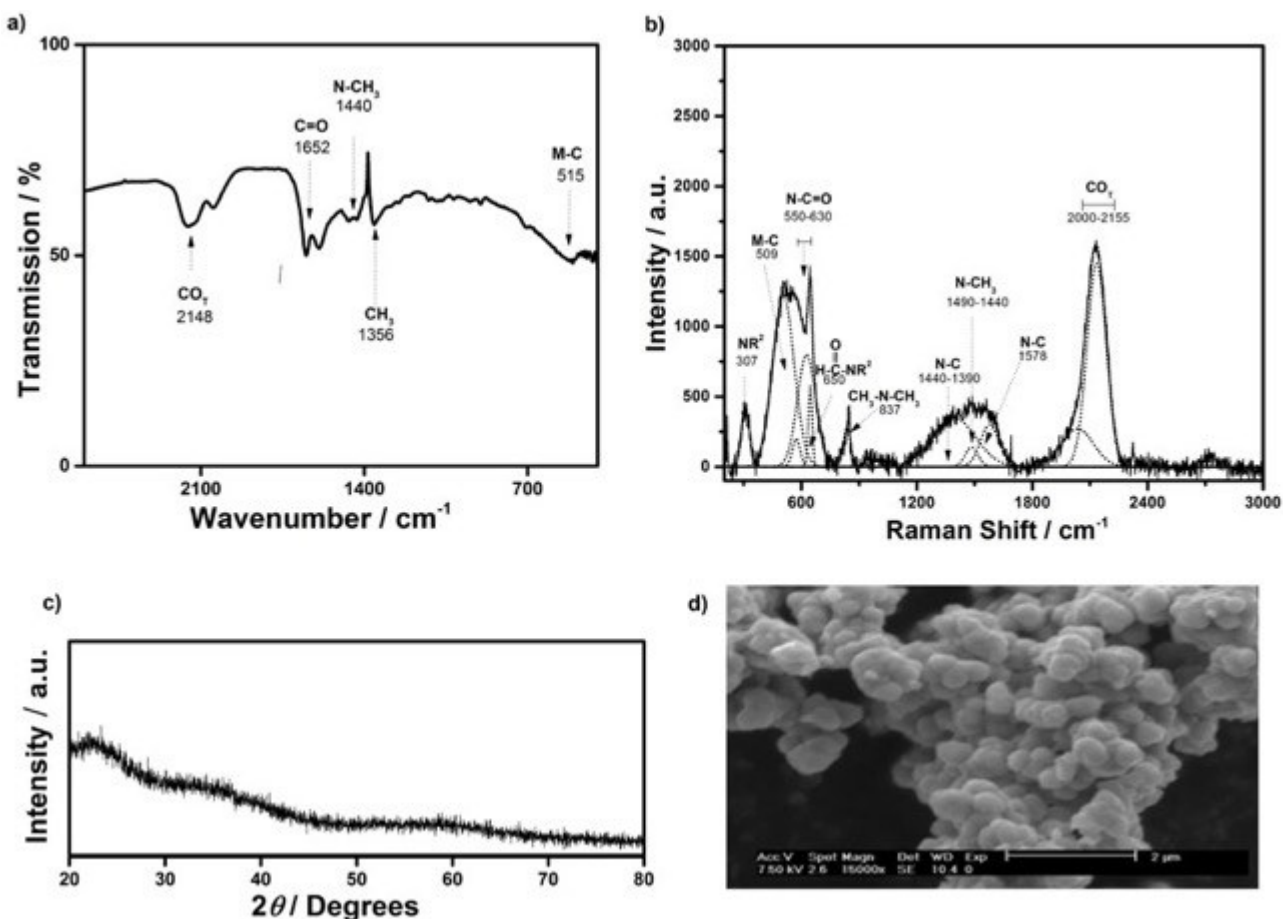


Figure 1. Structural characterization of $\text{Ir}_x\text{Mn}_y(\text{CO})_n(\text{DMF})_z$: a) FT-IR spectrum, b) Raman spectrum (including its deconvolution), c) X-ray diffraction pattern, and d) SEM micrograph

15].

For example, the bimetallic materials $\text{Ru}_x\text{Ir}_y(\text{CO})_n$ and $\text{Rh}_x\text{Ir}_y(\text{CO})_n$ exhibit high catalytic activity for O_2 reduction and H_2 oxidation, with resistance to methanol and carbon monoxide, respectively [11]. In this work we report the catalytic activity of the novel bimetallic complex $\text{Ir}_x\text{Mn}_y(\text{CO})_n(\text{DMF})_z$ for the ORR and HOR, even in the presence of common fuel cell contaminants, such as CH_3OH and CO .

2. EXPERIMENTAL

2.1. Synthesis

The new bimetallic catalyst $\text{Ir}_x\text{Mn}_y(\text{CO})_n(\text{DMF})_z$ was synthesized by the thermolytic reaction of 23.74 mg (0.03 mmol) of $\text{MnCl}_2 \cdot 4\text{H}_2\text{O}$ (Aldrich) and 33.15 mg (0.12 mmol) of $\text{Ir}_4(\text{CO})_{12}$ (Aldrich) in N,N-dimethylformamide (J. T. Baker) at reflux temperature (189 °C), for 5 h. The products were centrifuged and washed with acetone (J. T. Baker) to eliminate precursor and solvent residues, and dried at room temperature.

2.2. Structural Characterization

The structural characterization of the new product was performed by diffuse reflectance FT-IR spectroscopy in a Perkin-Elmer-GX3

spectrometer (with samples dissolved in KBr); by X-ray diffraction on a Rigaku D/max-2100 diffractometer ($\text{CuK}_{\alpha 1}$ radiation, 1.5406 Å). Complementary micro-Raman studies were carried out on a LabRAM HR Evolution Raman spectrometer. The excitation frequency used in the experiment was the 488 nm blue line of an Ar laser operating with a power of 100 mW. The spectrum integration time was typically 180 seconds, averaging the recorded spectra over three successive measurements. A focal configuration of the Raman probe was adopted throughout the experiments, using a 50 x objective lens. The scanning electron micrographs, as well as the chemical composition, were obtained on a Philips XL30ESEM microscope with a coupled EDS system.

2.3. Preparation of the Electrode

The catalytic activity of the new material was studied by the rotating disk electrode (RDE) technique. The working electrode was prepared by mixing 1 mg of $\text{Ir}_x\text{Mn}_y(\text{CO})_n(\text{DMF})_z$, 1 mg of carbon powder (Vulcan® XC72R, Cabot) and 20 μL of a 5% Nafion®/isopropanol solution (Aldrich) in an ultrasonic bath. Subsequently, an aliquot of 3 μL of this mixture was taken and placed on the surface of a glassy carbon disk electrode (geometrical area 0.072 cm²) and dried at room temperature.

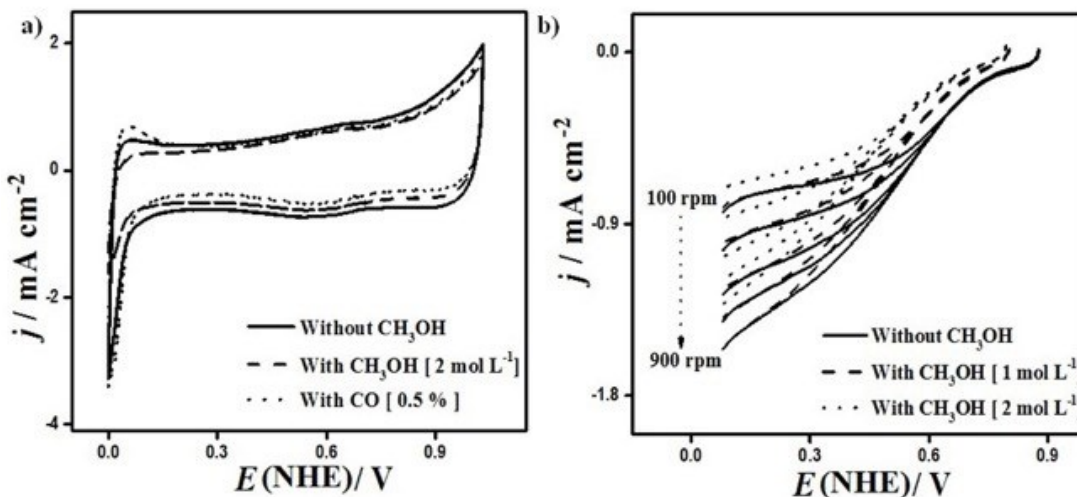


Figure 2. a) Cyclic voltammograms of $\text{Ir}_x\text{Mn}_y(\text{CO})_n(\text{DMF})_z$ in N_2 saturated $0.5 \text{ mol L}^{-1} \text{H}_2\text{SO}_4$, in the absence and presence of methanol (2.0 mol L^{-1}) and carbon monoxide (0.5%); the scan rate was 20 mV s^{-1} . b) Polarization curves of $\text{Ir}_x\text{Mn}_y(\text{CO})_n(\text{DMF})_z$ for oxygen reduction in $0.5 \text{ mol L}^{-1} \text{H}_2\text{SO}_4$, in the absence and presence of methanol in different concentrations; the sweep rate was 5 mV s^{-1} and the rotation rates were 100, 200, 400, 600 and 900 rpm

2.4. Electrochemical Characterization

2.4.1. Equipment

The RDE measurements were conducted at 25°C in a conventional electrochemical cell with three electrodes: a reference of mercury/mercury sulfate ($\text{Hg}/\text{HgSO}_4/0.5 \text{ mol L}^{-1}, \text{H}_2\text{SO}_4$; however, all the results are reported *vs.* the Normal Hydrogen Electrode), the working electrode and carbon cloth as the counter electrode. The electrolyte was $\text{H}_2\text{SO}_4 0.5 \text{ mol L}^{-1}$, prepared with 98% sulfuric acid (J.T. Baker) and deionized water ($18.3 \Omega \text{ cm}^{-1}$). A potentiostat/galvanostat (Princeton Applied Research, Model 263A) and a PC equipped with Echem-M270 software were used for the electrochemical measurements. A glassy carbon rotating disk electrode (BM-EDI101 Radiometer Analytical) and a speed control unit (CTV101) were used for the voltammetry studies.

2.4.2. Cyclic Voltammetry (CV)

Cyclic voltammetry was used to clean, activate and characterize the surface of the working electrode to perform the oxygen reduction and hydrogen oxidation reactions [16]. Before each measurement, the electrolyte was deoxygenated with nitrogen (Infra, UHP) for 15 min. The CV was performed by applying 30 potential sweeps from 0.0 to 1.03 V at a 20 mV s^{-1} scan rate.

2.4.3. Linear Sweep Voltammetry (LSV)

LSV was used to study the ORR and HOR. The polarization curves were obtained in three stages. The first stage was performed in O_2 or pure H_2 (Infra, UHP). For the ORR, oxygen (Infra, UHP) was bubbled in the electrolyte for 15 min, and the open circuit potential ($E_{\text{OC}}^{\text{O}_2}$) was measured. The polarization curves were obtained in the range ($E_{\text{OC}}^{\text{O}_2}$) to 0.1 V , at a 5 mV s^{-1} rate. The rotational speed was varied from 100 to 900 rpm. In the second and third stages of the ORR in the presence of methanol, the alcohol (JT Baker) was added to reach a final concentration of 1.0 or 2.0 mol L^{-1} and the

measurements were repeated. After each stage, the electrolyte was deoxygenated with nitrogen (for 15 min) to avoid changes in the concentration of the electroactive species inside the cell.

For the HOR, hydrogen (Infra, UHP) was bubbled in the electrolyte for 15 min. The current-potential curves were obtained from

$E_{\text{OC}}^{\text{H}_2}$ to 0.48 V at a 10 mV s^{-1} rate. The rotation speed ranged from 100 to 900 rpm. In the case of the HOR in the presence of carbon monoxide, mixtures of H_2/CO , with CO concentrations of 100 ppm and 0.5% (Infra, UHP), were bubbled for 15 min into the cell for the measurements. After each stage, the electrolyte was deoxygenated with nitrogen for 15 min.

3. RESULTS AND DISCUSSION

3.1. Structural Characterization

Figure 1 shows the FT-IR and micro-Raman spectra, the X-ray diffraction pattern and a SEM micrograph of the $\text{Ir}_x\text{Mn}_y(\text{CO})_n(\text{DMF})_z$ electrocatalyst. The FT-IR spectrum (Figure 1a) shows the band associated with the terminal carbonyl group at 2148 cm^{-1} . The bands observed around 1652 , 1440 and 1356 cm^{-1} correspond to the C=O , $\text{N}-\text{CH}_3$ and CH_3 groups of a tertiary amide [17] and are related to the reaction medium (N,N-DMF). The small band around 515 cm^{-1} could be due to vibration modes of $\text{v}(\text{MC})$ and/or $\partial(\text{MCO})$ [18]. The micro-Raman spectrum (Figure 1b) clearly shows the carbonyl stretching vibration band at $\sim 2000-2150 \text{ cm}^{-1}$. Upon deconvolution, the spectrum also shows the $\text{N}-\text{CH}_3$ and M-C

Table 1. Chemical composition of the $\text{Ir}_x\text{Mn}_y(\text{CO})_n(\text{DMF})_z$ electrocatalyst, obtained by EDS.

	Element (%W)					
	Ir	Mn	C	O	N	Cl
$\text{Ir}_x\text{Mn}_y(\text{CO})_n(\text{DMF})_z$	59.50	4.18	14.13	11.16	7.23	3.78

bands at 1440 and 509 cm⁻¹, respectively [19]. The deconvolution process also reveals bands associated with the HCO-NR², NR² and NC groups at 650, 837 and 1578 cm⁻¹, respectively. These bands are related with functional groups of a tertiary amide [20]. Additionally, a band involving NCO vibration modes of amide III is observed around 550-630 cm⁻¹ [21]. Table 1 shows the chemical composition of the new electrocatalyst; it can be observed that not only the four elements expected for the bimetallic carbonyl Ir_xMn_y(CO)_n are present, but also nitrogen and chlorine from the reaction medium and the manganese precursor, respectively. The N,N-DMF molecules are possibly coordinated to the metal centers due to their electron donor nature. Hence, the formulation Ir_xMn_y(CO)_n(DMF)_z is more representative of the novel catalytic material. The XRD pattern (Figure 1c) shows only broad features, a fact related with a small particle size of the sample, possibly in the nano regime. A SEM micrograph of the novel catalyst (Figure 1d) shows that it is formed by nearly round shape aggregates (average size = 470 nm).

3.2. Electrochemical Characterization

3.2.1. Cyclic Voltammetry

Figure 2a shows the cyclic voltammograms of Ir_xMn_y(CO)_n(DMF)_z in H₂SO₄ 0.5 mol L⁻¹, both with and without methanol (2.0 mol L⁻¹). The cyclic voltammogram of the novel electrocatalyst in the presence of an H₂/CO mixture ([CO] = 0.5%) is shown as well. The cyclic voltammograms in the absence of methanol show a hydrogen evolution zone between 0 and 0.2 V, anodic-cathodic peaks in the 0.5-0.7 V range, ascribed to the Vulcan® support, and a peak associated with oxygen evolution (anodic region between 0.9 and 1.0 V). In the presence of methanol (2 mol L⁻¹), the novel electrocatalyst shows a small decrease in the intensity of the peak related to the hydrogen evolution reaction.

On the other hand, the cyclic voltammograms basically exhibit the same features in the presence of carbon monoxide, indicating the material's tolerance to such contaminant. No peaks associated with the oxidation of methanol or carbon monoxide are observed, in contrast with Pt, which easily oxidizes both compounds [22, 23].

3.2.2. Linear Sweep Voltammetry: Oxygen Reduction Reaction (ORR)

The curves for the electrochemical reduction of molecular oxygen on Ir_xMn_y(CO)_n(DMF)_z, in 0.5 mol L⁻¹ sulfuric acid, are shown in Figure 2b; the polarization curves in the presence of methanol in two concentrations are shown as well. The curves show the three characteristic zones of ORR processes taking place on a catalyst's surface: (I) the kinetic zone (~0.8-0.7 V), where the current i_k is independent of the rotation velocity; (II) the mixed control zone (~0.7-0.55 V), where the behavior is determined by kinetic as well as diffusion processes; and (III) the mass-transfer zone (~0.55-0.1 V), where the diffusion current, i_d , is a function of the rotation velocity. The polarization curves do not show significant changes in the presence of methanol, which confirms the tolerance properties of the novel electrocatalyst to perform the oxygen reduction reaction in the presence of this contaminant [24, 25].

The analysis of the catalytic currents as a function of the rotation rate uses the Koutecky-Levich Equation [26]:

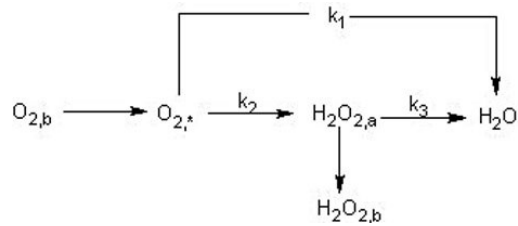


Figure 3. Proposed model for oxygen reduction in an aqueous electrolyte: a, adsorbed on the electrode surface; *, in the vicinity of the electrode surface; b, in bulk solution

$$\frac{1}{i} = \frac{1}{i_k} + \frac{1}{B\omega^{1/2}} \quad (1)$$

where i denotes the total current density (mA cm⁻²), i_k is the kinetic current (mA cm⁻²), ω the rotation rate (rpm) and B the Levich constant, which is defined in Equation (2):

$$B = 0.62nFAC_{O_2}(D_{O_2})^{2/3}\nu^{-1/6} \quad (2)$$

where n is the electron transfer number, F the Faraday constant (96 485 C mol⁻¹), A the geometrical area of the electrode (0.072 cm²), C_{O_2} the concentration of O₂ ($1.1 \times 10^{-6} \text{ mol cm}^{-3}$) in solution, D_{O_2} is the O₂ diffusion coefficient ($1.4 \times 10^{-5} \text{ cm}^2 \text{ s}^{-1}$) in the electrolyte and ν the kinematic viscosity of the solution ($0.01 \text{ cm}^2 \text{ s}^{-1}$) [27].

This equation is useful to indicate the two different reaction pathways that the catalyst could use to perform the oxygen reduction reaction. There are various reaction schemes proposed for the ORR [28]. The simple model proposed by Damjanovic *et al.* [29] is presented in Figure 3, where k_1 , k_2 and k_3 are the rate constants. This model assumes: (I) the direct reduction of oxygen to water involving a 4-electron charge transfer process; (II) a serial mechanism in which the reduction of oxygen to hydrogen peroxide is followed by reduction to water. The best mechanism for a PEMFC is the 4-electron route, since the generation of H₂O₂ in the cell is highly undesirable as it diffuses into the PEM and results in radical oxidative degradation of the membrane [30]. Moreover, the chemical reactions are faster and the process is more efficient [31].

Figure 4a shows experimental (at a given potential value) and theoretical (2 and 4 electron) Koutecky-Levich plots. The experimental plots are closer to the plots calculated for a 4-electron process, than to those for a 2-electron pathway. Additionally, the value of the Koutecky-Levich slope calculated for the bimetallic electrocatalyst ($78.2 \text{ rpm}^{1/2} \text{ mA}^{-1}$) is closer to the magnitude of the slope for a 4-electron mechanism ($132.7 \text{ rpm}^{1/2} \text{ mA}^{-1}$) than to that for $n = 2$ ($265.41 \text{ rpm}^{1/2} \text{ mA}^{-1}$). This analysis suggests that O₂ is directly reduced to H₂O in a four-electron process, even in the presence of methanol. The effective area was calculated with the experimental Koutecky-Levich slope and $n=4$; all the currents reported were normalized to this effective area. The open circuit potential shown by the bimetallic electrocatalyst, 0.878 V, was higher than that exhibited by the iridium precursor under the same conditions, 0.8 V [32]. Figure 4b shows the reaction order, m , calculated from the

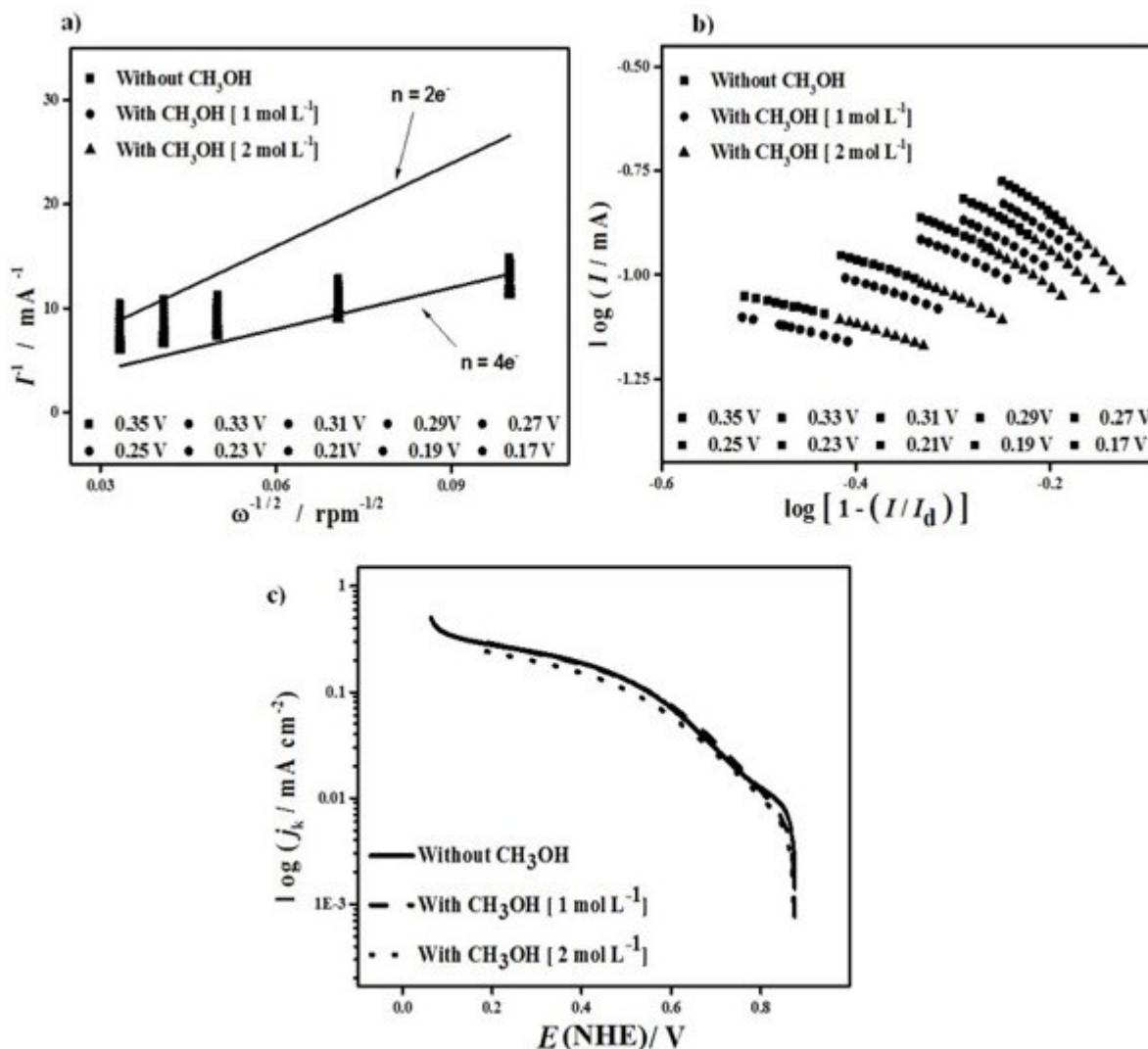


Figure 4. a) Experimental (at a given V value) and theoretical (2 and 4 electrons) Koutecky-Levich plots, b) $\log I$ vs. $\log [1 - (I/I_d)]$ plots for several rotation rates (at a given V value), and c) ORR mass-transfer corrected Tafel plots for $\text{Ir}_x\text{Mn}_y(\text{CO})_n(\text{DMF})_z$, in the absence and presence of methanol (1.0 and 2.0 mol L⁻¹)

slope of the $\log I$ vs. $\log [1 - (I/I_d)]$ plots for different rotation speeds at a given potential. The value calculated for m is virtually one with respect to dissolved O_2 in the electrolyte; moreover, such value is practically unaffected by the presence of methanol (average values are shown in Table 2). The mass transfer corrected Tafel plots are

shown in Figure 4c for $\text{Ir}_x\text{Mn}_y(\text{CO})_n(\text{DMF})_z$ for the molecular oxygen reduction reaction at 25 °C.

The kinetic parameters (obtained from the Tafel plots) of the novel bimetallic catalyst, such as Tafel slope (b), exchange current density (j_0) and charge transfer coefficient (α) were derived from

Table 2. Open circuit potential and kinetic parameters of $\text{Ir}_x\text{Mn}_y(\text{CO})_n(\text{DMF})_z$ for the oxygen reduction reaction (ORR), in the absence and presence of methanol.

	[MeOH] (mol L ⁻¹)	$E_{\text{OC}}^{\text{O}_2}$ (V)	m	b (mV dec ⁻¹)	α	j_0 (mA cm ⁻²)
$\text{Ir}_x\text{Mn}_y(\text{CO})_n(\text{DMF})_z$	0	0.878	1	246.55	0.24	1.72×10^{-3}
	1	0.804	1	224.25	0.27	6.31×10^{-4}
	2	0.795	1	240.12	0.25	6.27×10^{-4}

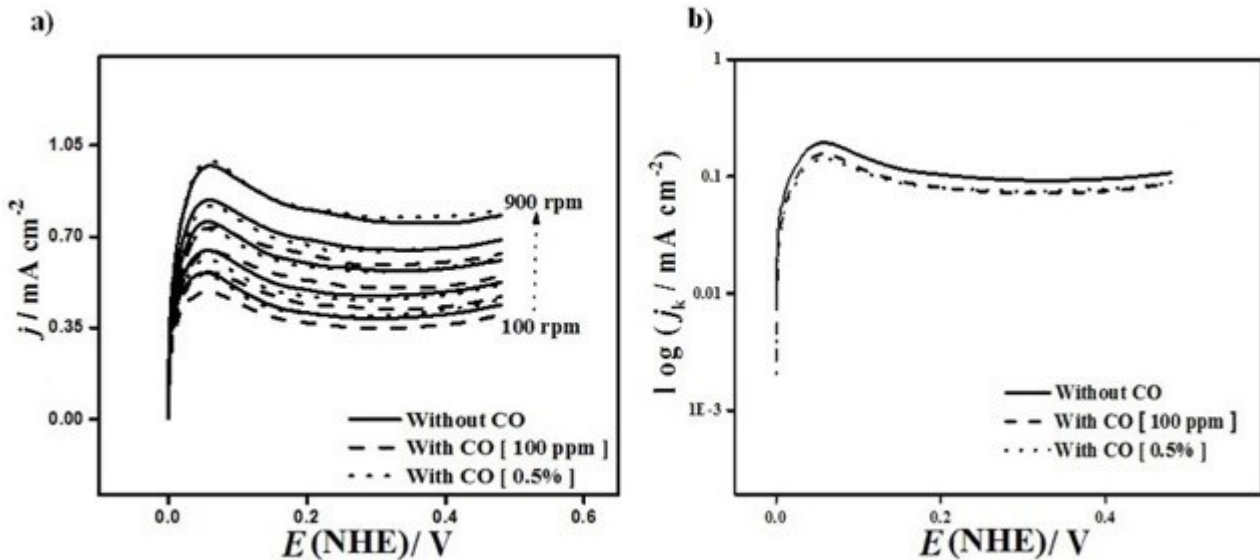


Figure 5. Polarization curves of $\text{Ir}_x\text{Mn}_y(\text{CO})_n(\text{DMF})_z$ for hydrogen oxidation in 0.5 mol L^{-1} H_2SO_4 , in the absence and presence of carbon monoxide in different concentrations; the sweep rate was 10 mV s^{-1} and the rotation rates were 100, 200, 400, 600 and 900 rpm. b) HOR mass-transfer corrected Tafel plots for $\text{Ir}_x\text{Mn}_y(\text{CO})_n(\text{DMF})_z$ with and without carbon monoxide

equation (3) and the Tafel slopes from equation (4),

$$i_k = \frac{i * i_d}{i_d - i} \quad (3)$$

$$\eta = a + b \log |i_k| \quad (4)$$

in which i , i_k and i_d are the overall, kinetic and diffusion-limiting current, respectively. The semilogarithmic equation is known as the Tafel equation and b is the so-called Tafel slope. In the high overpotential region ($E > 0.6 \text{ V}$), the Tafel slope values were around $2.3RT(\alpha F)^{-1}$ [33]. The kinetic parameters for the $\text{Ir}_x\text{Mn}_y(\text{CO})_n(\text{DMF})_z$ catalyst have been assembled in Table 2. It can be observed that the values of Tafel slopes calculated are significantly higher (av. 237 mV dec^{-1}) than the magnitudes reported for Pt/Vulcan® and $\text{Ir}_4(\text{CO})_{12}/\text{Vulcan}^\circledR$, 78.12 [34] and $118.00 \text{ mV dec}^{-1}$ [32], respectively. This result suggests that the reaction mechanism is different for the three materials. The parameter related with the free energy of activation of an electrochemical process, α (av. 0.25) [35], decreases with respect to the values reported for Pt and $\text{Ir}_4(\text{CO})_{12}$, 0.75 and 0.50, respectively [32, 34]. One of the most important kinetic parameters is the exchange current density (j_0). This parameter gives information about the electronic transfer velocity, *i.e.* how fast the ORR is carried out [35]. The exchange current density values obtained for $\text{Ir}_x\text{Mn}_y(\text{CO})_n(\text{DMF})_z$ in the absence of methanol ($1.72 \times 10^{-3} \text{ mA cm}^{-2}$) are three orders of magnitude higher than those found for Pt/Vulcan® and two orders than those for $\text{Ir}_4(\text{CO})_{12}/\text{Vulcan}^\circledR$ (1.4×10^{-6} and $1.89 \times 10^{-5} \text{ mA cm}^{-2}$, respectively) [32, 34]. Although the j_0 values decrease *ca.* an order of magnitude in the presence of methanol, the other kinetic parameters presented in Table 2 do not show significant changes. Therefore, the novel catalyst shows a high selectivity to oxygen and it is able to reduce it in the presence of a DMFC cathode contaminant such

as methanol. The bimetallic material resists the presence of methanol even to a concentration of 2 mol L^{-1} , above the tolerance levels of other catalysts, which are usually resistant to methanol concentrations of 1 mol L^{-1} [36-41].

In this work a new bimetallic electrocatalyst was obtained from the thermolytic reaction of a noble metal carbonyl complex and a salt of a first-row transition metal; this compound is innovative as it replaces platinum and adds a non-noble transition metal. On the basis of the results obtained it was observed that the properties of the bimetallic complex improved in some aspects, compared with the monometallic carbonyl precursor [32]. This behavior can be usually ascribed to two effects, or a combination of them: the bi-functional effect, in which the catalytic properties of each of the elements in the material combine in a synergetic way to yield a surface which is more active than each of the individual elements, and the ligand or electronic effect, in which one of the elements modifies the electronic properties of the other to yield a more active catalytic surface [42, 43]. The latter effect seems to be operating in the present case, *i.e.* the manganese atoms enhancing the catalytic activity of the iridium metal core.

3.2.3. Linear Sweep Voltammetry: Hydrogen Oxidation Reaction (HOR)

Figure 5a shows the current-potential curves of $\text{Ir}_x\text{Mn}_y(\text{CO})_n(\text{DMF})_z$ for hydrogen oxidation in 0.5 mol L^{-1} H_2SO_4 , in absence and presence of CO ([CO] = 100 ppm and 0.5%), at different rotation rates (100-900 rpm). Figure 5b shows the HOR mass-transfer corrected Tafel plots for $\text{Ir}_x\text{Mn}_y(\text{CO})_n(\text{DMF})_z$ with and without carbon monoxide. The electrooxidation curves practically do not change in the presence of carbon monoxide, thus indicating the important resistance properties of the bimetallic catalyst to this contaminant. The kinetic parameters were obtained from the mass transfer corrected Tafel plots shown in Figure 5b and the

results are summarized in Table 3.

As in the case of the ORR, the Tafel slope is related to the reaction pathway. For the HOR, the Tafel slope values were calculated to be around $2.3RT/(1-\alpha)F$ [33]. Mello and Ticianelli have proposed different mechanisms for a catalyst to carry out the HOR, mainly on the basis of the Tafel slope value [44].

In this work, the value obtained for b was $\sim 62 \text{ mV dec}^{-1}$ with pure hydrogen, suggesting an irreversible direct discharge mechanism:



When hydrogen and CO are both present, the mechanism does not appear to change, since the value of b is practically maintained. The calculated α values (av. 0.97) are close to that reported for Pt (1.0) [45], thus indicating a similar energy requirement for the reaction to proceed.

The magnitude of the exchange current density (j_0) of $\text{Ir}_x\text{Mn}_y(\text{CO})_n(\text{DMF})_z$ for the HOR in the absence of CO (0.685 mA cm^{-2}) is higher than those found for Pt/Vulcan® (0.47 mA cm^{-2}) [34] and $\text{Ir}_4(\text{CO})_{12}/\text{Vulcan}^\circledR$ ($0.1231 \text{ mA cm}^{-2}$) [32]. Moreover, its value is not significantly affected by the presence of carbon monoxide in both concentrations, showing the tolerance of the bimetallic complex to this contaminant. These results are in agreement with those of the cyclic voltammetry studies, where no peaks of CO oxidation were detected, thus confirming the high selectivity of the present catalyst to the hydrogen oxidation process. This property is a very important advantage over platinum-based catalysts, since the latter are easily deactivated by CO concentrations of a few ppm [46, 47].

The kinetic parameters of Table 3, specially the fact that the exchange current densities of the bimetallic catalyst are considerably higher (by a factor of 6) than those of the monometallic precursor $\text{Ir}_4(\text{CO})_{12}$ [32], again brings forth the matter of an enhancement of the catalytic properties of the iridium cluster by the presence of manganese, through electronic effects occurring in the metal atom core.

It is interesting to note that such an enhancement is observed even at a low concentration of manganese (~4%), which naturally leads to doing further investigation of other bimetallic complexes with higher concentrations of this metal, as well as to perform additional studies for a better understanding of the mechanism through which this effect is taking place.

4. CONCLUSIONS

In this work we report a novel bimetallic electrocatalyst, $\text{Ir}_x\text{Mn}_y(\text{CO})_n(\text{DMF})_z$, that performs both the oxygen reduction and hydrogen oxidation reactions in $0.5 \text{ mol L}^{-1} \text{ H}_2\text{SO}_4$, showing a dual

behavior. The $\text{Ir}_x\text{Mn}_y(\text{CO})_n(\text{DMF})_z$ catalyst is innovative as it replaces platinum and adds a non-noble transition metal. The improvement in some important parameters of both reactions, with respect to the monometallic iridium precursor, are probably explained in terms of an electronic factor induced by the presence of manganese in the mixed metal atom core. The resulting surface exhibits enhanced catalytic properties compared to the monometallic $\text{Ir}_4(\text{CO})_{12}$ cluster. In addition, the novel electrocatalyst is tolerant to significant levels of common fuel cell contaminants such as methanol and carbon monoxide in the ORR and HOR, respectively. This is an important advantage over traditional platinum catalysts, since the latter are easily deactivated by low concentrations of such contaminants. Therefore, the catalyst reported in this work is attractive for evaluation as cathode in DMFC and as anode in reforming hydrogen PEM fuel cells. The results of the present investigation are also encouraging to continue the work of incorporating non-noble transition metals into the structure of platinum group metal complexes, with the possibility of attaining enhanced activities as catalysts for fuel cells, with a concomitant lower cost.

5. ACKNOWLEDGMENTS

The authors thank M. A. Hernández-Landaverde, J. E. Urbina-Alvarez, A. Jiménez-Prieto, F. Rodríguez-Melgarejo and R. A. Mauricio-Sánchez for technical support. The authors are grateful to CONACYT for grant No. 224366 and for a graduate scholarship to M. L. Barrios-Reyna.

REFERENCES

- [1] Barbir F., PEM Fuel Cell Theory and Practice, Elsevier, San Diego, 2005.
- [2] Ralph T.R., Horgarth M.P., Platinum Met. Rev., 46, 3 (2002).
- [3] Li X., Principles of Fuel Cells, Taylor & Francis, New York, 2006.
- [4] Horgarth M.P., Ralph T.R., Platinum Met. Rev., 46, 146 (2002).
- [5] Stamenkovic V., Mun B.S., Mayrhofer K.J.J., Ross P.N., Markovic N.M., Rossmeisl J., Greeley J., Nørskov J.K., Angew. Chem. Int. Ed., 45, 2897 (2006).
- [6] Ermete A., Appl. Catal. B Environ., 74, 337 (2007).
- [7] Wang R.F., Liao S.J., Liu H.Y., Meng H., J. Power Sources, 171, 471 (2007).
- [8] Mojovic Z., Mudrinic T., Rabi-Stankovic A., Ivanovic-Sasic A., Marinovic S., Zunic M., Jovanovic D., Sci. Sinter., 45, 89 (2013).
- [9] Lefterova E.D., Stoyanova A.E., Borisov G.R., Slavcheva E.P., Bulg. Chem. Commun., 43, 138 (2011).

Table 3 Open circuit potential and kinetic parameters of $\text{Ir}_x\text{Mn}_y(\text{CO})_n(\text{DMF})_z$ for the hydrogen oxidation reaction (HOR), in the absence and presence of carbon monoxide.

	[CO]	$E_{\text{OC}}^{\text{H}_2}$ (V)	b (mV dec $^{-1}$)	α	j_0 (mA cm $^{-2}$)
$\text{Ir}_x\text{Mn}_y(\text{CO})_n(\text{DMF})_z$	0	0	62.52	0.96	0.685
	100 ppm	0	61.71	0.97	0.524
	0.5%	0	60.34	0.99	0.585

- [10]Lima F.H.B., Calegaro M.L., Ticianelli E.A., *Electrochim. Acta*, 52, 3732 (2007).
- [11]Hernández-Hernández H.M., Olivares-Ramírez J.M., Jiménez-Sandoval O., *Int. J. Hydrogen Energy*, 38, 7674 (2013).
- [12]Jang I., Hwang I., Tak Y., *Electrochim. Acta*, 90, 148 (2013).
- [13]Marshall A., Borresen B., Hagen G., Tsyplkin M., Tunold R., *Electrochim. Acta*, 51, 3161 (2006).
- [14]Siracusano S., Baglio V., Di Blasi A., Briguglio N., Stassi A., Ornelas R., Trifoni E., Antonucci V., Aricò A.S., *Int. J. Hydrogen Energy*, 35, 5558 (2010).
- [15]Radev I., Topalov G., Lefterova E., Ganske G., Schnakenberg U., Tsotridis G., Slavcheva E., *Int. J. Hydrogen Energy*, 37, 7730 (2012).
- [16]Willard H., Dean J., Merrit Jr. L., Settle J.r F.A., *Instrumental Methods of Analysis*, Van Nostrand, New York, 1981.
- [17]Chalmers J.M., Griffiths P.R., *Handbook of Vibrational Spectroscopy*, Wiley, West Sussex, 2002.
- [18]Nakamoto K., *Infrared and Raman Spectra of Inorganic and Coordination Compounds, Part B: Applications in Coordination, Organometallic and Bioinorganic Chemistry*, Wiley, New York, 2009.
- [19]Lin Vien D., Colthup N.B., Fateley W.G., Grasselli J.G., *Handbook of Infrared and Raman Characteristic Frequencies of Organic Molecules*, Academic Press, San Diego, 2002.
- [20]Desseyen H.O., Herrebout W.A., Clou K., *Spectrochim. Acta A*, 59, 835 (2003).
- [21]Dollish F.R., Fateley W.G., Bentley F.F., *Characteristic Raman Frequencies of Organic Compounds*, Wiley, New York, 1974.
- [22]Shukla A.K., Raman R.K., *Annu. Rev. Mater. Res.*, 33, 155 (2003).
- [23]Gasteiger H.A.H., Markovic N.M., Ross P.N., *J. Phys. Chem.*, 99, 8290 (1995).
- [24]Gojkovic S.L., Vidakovic T.R., *Electrochim. Acta*, 47, 633 (2001).
- [25]Altamirano-Gutiérrez A., Jiménez-Sandoval O., Uribe-Godínez J., Castellanos R.H., Borja-Arco E., Olivares-Ramirez J.M., *Int. J. Hydrogen Energy*, 34, 7983 (2009).
- [26]Cheon J.Y., Ahn C., You D.J., Pak C., Hur S.H., Kim J., Joo S.H., *J. Mater. Chem. A*, 1, 1270 (2013).
- [27]Alonso-Vante N., Tributsch H., Solorza-Feria O., *Electrochim. Acta*, 40, 567 (1995).
- [28]Kinoshita K., *Electrochemical Oxygen Technology*, Wiley, New York, 1992.
- [29]Damjanovic A., Genshaw M.A., Bockris J., *J. Chem. Phys.*, 45, 4057 (1996).
- [30]Borup R., Meyers J., Pivovar B., Kim Y.S., Mukundan R., Garland N., Myers D., Wilson M., Garzon F., Wood D., Zelenay P., More K., Stroh K., Zawodzinski T., Boncella J., McGrath J.E., Inaba M., Miyatake K., Hori M., Ota K., Ogumi Z., Miyata S., Nishikata A., Siroma Z., Uchimoto Y., Yasuda K., Kimijima K.I., Iwashita N., *Chem. Rev.*, 107, 3904 (2007).
- [31]Hsueh K.L., Chin D.T., Srinivasan S., *J. Electroanal. Chem.*, 153, 79 (1983).
- [32]Uribe-Godínez J., Jiménez-Sandoval O., *Int. J. Hydrogen Energy*, 37, 9477 (2012).
- [33]Gileadi E., *Electrode Kinetics*, Wiley, New York, 1993.
- [34]Borja-Arco E., Castellanos R.H., Uribe-Godínez J., Altamirano-Gutiérrez A., Jiménez-Sandoval O., *J. Power Sources*, 188, 387 (2009).
- [35]Bard A.J., Faulkner L.R., Swain E., Robey C., *Electrochemical Methods: Fundamentals and Applications*, Wiley, New York, 2001.
- [36]Chu D., Jiang R., *Solid State Ionics*, 148, 591 (2002).
- [37]Tributsch H., Bron M., Hilgendorff M., Schulenburg H., Dorbandt I., Eyert V., Bogdanoff P., Fiechter S., *J. Electroanal. Chem.*, 8, 739 (2001).
- [38]Jiang R.Z., Chu D., *J. Electrochem. Soc.*, 147, 4605 (2000).
- [39]Ocampo A.L., Castellanos R.H., Sebastian P.J., *J. New Mater. Electrochem. Syst.*, 5, 163 (2002).
- [40]Hilgendorff M., Diesner K., Schulenburg H., Bogdanoff P., Bron M., Fiechter S., *J. New Mater. Electrochem. Syst.*, 5, 71 (2002).
- [41]Sun G.Q., Wang J.T., Savinell R.F., *J. Appl. Electrochem.*, 28, 1087 (1998).
- [42]Schmidt T.J., Paulus U.A., Gasteiger H.A., Alonso-Vante N., Behm R.J., *J. Electrochem. Soc.*, 147, 2620, 2000.
- [43]Koper M.T.M., *Surf. Sci.*, 548, 1 (2004).
- [44]Mello R.M.Q., Ticianelli E.A., *Electrochim. Acta*, 42, 1031 (1997).
- [45]Uribe-Godínez J., García-Montalvo V., Jiménez-Sandoval O., *Int. J. Hydrogen Energy*, 38, 7680 (2013).
- [46]Urián R.C., Gullá A.F., Mukerjee S., *J. Electroanal. Chem.*, 554-555, 307 (2003).
- [47]Lopes P.P., Freitas K.S., Ticianelli E.A., *Electrocatalysis*, 1, 200, 2010.